Fluid Flow and Solute Transport in a Single Fracture with Variable Apertures under the Normal Compliance Effect

○Jeong, Woo-Chang[1], Song, Jai-Woo

1. Introduction

Faults and fractures play an important role in the transport of fluid and solute through rocks with low permeability. Under a wide range of circumstances these transport processes are concentrated onto a network of interconnected fractures. Thus, it is important to understand the properties of fluid flow and solute transport in individual fractures that consist of a fracture network.

Under effective normal stress, fracture walls create a complex distribution of contact and open areas, which have significant effects on fluid flow and solute transport. In this paper, we presented numerical studies of the behaviors of fluid flow and solute transport in a single fracture loaded by effective normal stress. Apertures are distributed in a single fracture by a Gaussian law and the roughness of fracture surfaces are represented by using a self-affine fractal model. The solute transport simulation was performed by using the particle following method (Jeong and Song, 1998).

2. Generation of variable apertures in a single fracture

Fluid flow in a natural single fracture is sensible to the distribution of variable apertures (Gentier, 1986; Brown, 1987). Most of measures detailed for the aperture distribution are performed by laboratory experiments with natural fracture samples (Hakami and Barton, 1990). According to their results, the apertures between two walls of fracture are distributed by a log-normal or gaussian law. This type of apertures has been used in most of numerical and analytical studies of the fluid flow and the solute transport in single fractures with variable apertures (Moreno *et al.*, 1988; Pyrak-Nolte *et al.*, 1988; Renshaw, 1995).

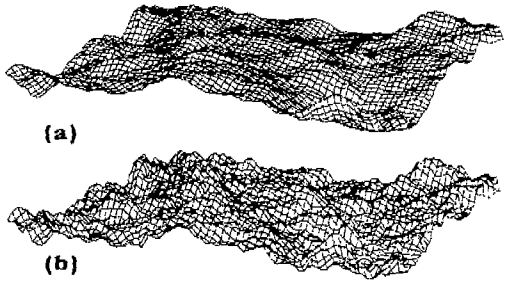

Fig.1. Fractal surface generated using a Fourier filtering algorithm on a lattice of size 64 × 64. (a) D = 2.0, (b) D = 2.5.

In this study, variable apertures in a single fracture are normally distributed and the roughness of fracture surface is represented by using a self-affine fractal model (Meakin *et al.*, 1997). The self-affine fractal surface is characterized by its fractal dimension D and looks '*similar to itself*' when the length scales in the x- and y-direction are rescaled by a factor b and the length scale in the z direction is rescaled simultaneously by the factor $b^{\prime}$. Fig. 1 illustrates an example of fractal surface generated on a lattice of size 64×64 by using two different values of D. We can see that the fractal surface with $D = 2.0$ is more smooth than that with $D = 2.5$.

[1] Researcher, Research Center for Disaster Prevention and Safety Management, Hong-Ik University
[2] Professor, Department of Civil Engineering, Hong-Ik University

3. Local fluid flow model at single fracture scale

Once the variable apertures are generated in a single fracture discretized into square grids, each cell of size Δa being characterized by its own aperture e, the local flow can be calculated by taking the following hypotheses: 1) fluid flow takes place in laminar range, 2) the cubic law is locally valid at the fracture cell's scale. The hydraulic conductivity between cells i and j is calculated as harmonic mean. The volumetric flow rate Q between cells i and j with apertures e_i and e_j respectively is then proportional to the hydraulic head gradient, as follows:

$$Q_{ij} = \frac{g}{12\nu} \frac{2\Delta a}{\left(\frac{1}{e_i^3} + \frac{1}{e_j^3} \right)} \left(\frac{h_i - h_j}{\Delta a} \right) \tag{1}$$

where $g[ms^{-2}]$ denotes a gravitational acceleration, $\nu[m^2s^{-1}]$ is a cinematic viscosity and h_i and h_j are hydraulic heads at cells i and j respectively.

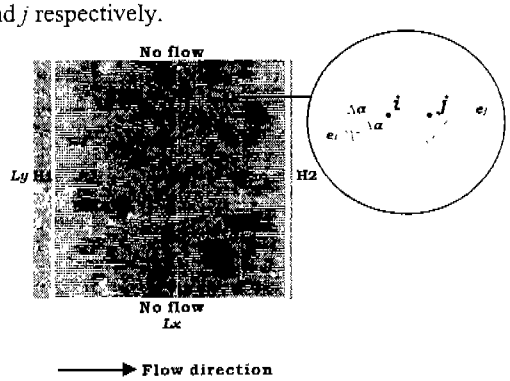

Fig.2. Schematic illustration of fluid flow through a single fracture with variable apertures. H1 and H2 are the global hydraulic heads prescribed at two opposite boundaries (H1 > H2).

In a steady-state flow condition, the principle of mass conservation at node i connecting to j other nodes can be written as the following equation:

$$\sum_j Q_{ij} = 0 \tag{2}$$

After prescribed unit hydraulic heads (1 *m/m*) at two opposite boundaries (Fig. 2), the equation (2) can be solved for the global flow in a single fracture. No flow condition is imposed at two boundaries parallel to the flow direction.

3. Solute transport model at single fracture scale

Once the steady-state flow is numerically solved, the transport simulation through the single fracture will be carried out using the particle following algorithm. Particles are randomly introduced along the upstream boundary, as a line source. When particles arrive at intersection, they reorient toward one of out-going branches with a sampling and a probability proportional to the local flow rate.

Assuming that particles are inert and that no matrix diffusion occurs, the mean residence time t_i of a particle in each square element i is calculated as follows:

$$t_i = \frac{V_i}{\sum_j Q_{ij}} = \frac{e_i \Delta a^2}{\sum_j Q_{ij}} \tag{3}$$

where e_i $[m]$ is an aperture of element i and V_i $[m^3]$ is a volume of element i.

The summation of these mean residence times along channels from the upstream boundary to downstream boundary gives the total residence time of the particle. This calculation repeats for many particles (for example, 10000) and the result obtained is represented by a breakthrough curve on the downstream boundary.

4. Hydromechanical coupling at the single fracture scale

Fluid flow in a rough fracture depends strongly on the aperture distribution. This distribution may be varied with effective normal stress applied. As consequence, the effect of normal stress can influence the fluid flow and solute transport in a single fracture. Generally, the relationship between the fracture aperture and the supported effective normal stress is non-linear (Bandis *et al.*, 1983). In this study, we used Bandis' hyperbolic model, which is expressed by:

$$\sigma_n' = \frac{k_{n0}\Delta u e_0}{e_0 + \Delta u} \tag{4}$$

where k_{n0} $[MPam^{-1}]$ is the normal stiffness at effective normal stress of zero, e_0 $[m]$ is the maximum closure (*i.e.* initial value of aperture in a unloaded condition) and Δu $[m]$ is the closure displacement.

Values of parameter of Bandis' model used in this numerical study are listed in Table 1. These values are obtained from various hydraulic tests performed in the geothermic research area of Soult-sous-Forêt in France.

Table 1. Parameters and its values used in a numerical simulation

Parameters	Values
Initial mean aperture, e_0 $[\mu m]$	425.0
Standard deviation, σ_m $[\mu m]$	153.0
Initial normal stiffness, k_{n0} $[MPa\ m^{-1}]$	25000.0

In our numerical simulation, the closure is uniformly increased (Table 2) and we will investigate the transport behaviors of fluid and solute induced by this compliant effect.

Table 2. Values of Δu and corresponding σ_n' used in numerical simulations

Δu ($\times 10^{-4}$ m)	0.00	0.50	1.00	1.25	1.50	1.75	2.00	2.25	2.50	2.75	3.00	3.25
σ_n' (MPa)	0.00	1.42	3.27	4.43	5.80	7.44	9.44	11.95	15.18	19.48	25.50	34.53

5. Numerical results

5.1 Fluid flow simulation

Fluid flow simulations were carried out in 10 independent distributions at each level of effective normal stress and all of results that we will present corresponds to mean values for 10 realizations. As an example, Fig.3 illustrates the distributions of local flow rate for D = 2.5 and 2.0 at σ'_n = 9.44 *MPa*. The fluid flow in D = 2.5 is more tortuous than that in D = 2.0.

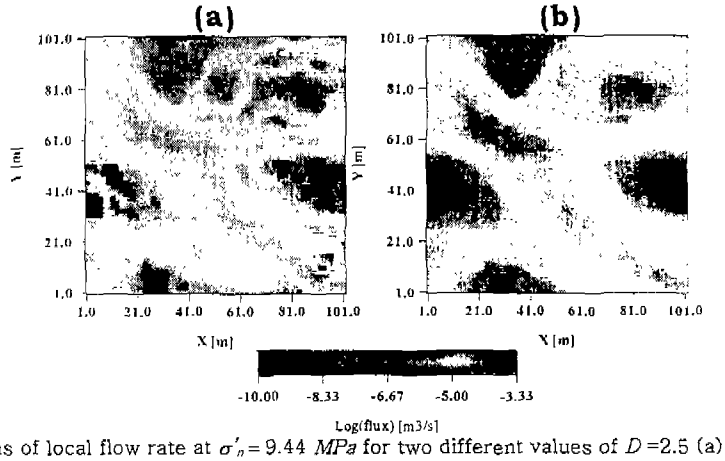

Fig. 3. Distributions of local flow rate at σ'_n = 9.44 *MPa* for two different values of D =2.5 (a) and 2.0 (b). Dark areas represent zones in contact.

Fig. 4 shows variations of the effective permeability of fracture with the effective normal stress for D = 2.50, 2.20 and 2.00. We can observe that the effective permeability decreases almost identically between

three values of D. However, the fracture generated by D = 2.00 is slightly more permeable than others. This phenomenon is due to the difference of roughness, which is varied with D. In general, more the fracture is rough, more its permeability decreases (Moreno *et al.*, 1988; Ewing and Jaynes, 1995).

The relationship between the effective permeability of fracture and the ratio of mean effective aperture (e_m) and its standard deviation (σ_m) is shown in Fig. 5. This ratio represents the mean separation between two walls in a rough fracture and can be considered as a measure of fracture roughness (Brown, 1987).

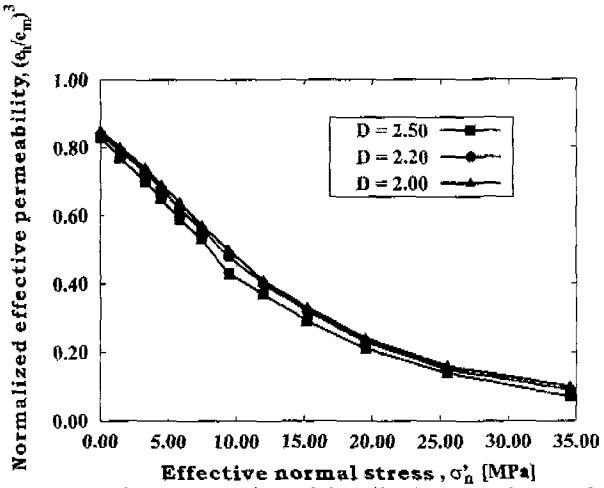

Fig. 4. Relationship between the effective permeability and the effective normal stress for three different values of D = 2.5, 2.2 and 2.0. The effective permeabilities are normalized by a value at σ'_n = 0.0. e_h is a hydraulic aperture calculated by *cubic law* and e_m is a mean effective aperture corresponding to a arithmetic average of apertures obtained from each level of the effective normal stress.

When the ratio of e_m and σ_m decreases, the effective permeability decreases showing almost identical tendency between D = 2.5, 2.2 and 2.0. This tendency of effective permeability is similar to that obtained from Thomson's work (1991). We also compared with results obtained from Zimmerman and Bodvarsson's empirical model (1996) which is expressed by:

$$\left(\frac{e_h}{e_m}\right)^3 = \left[1-1.5\left(\frac{\sigma_m}{e_m}\right)^2\right](1-2c) \tag{5}$$

where e_h [m] is a hydraulic aperture and c is a ratio of zones in contact.

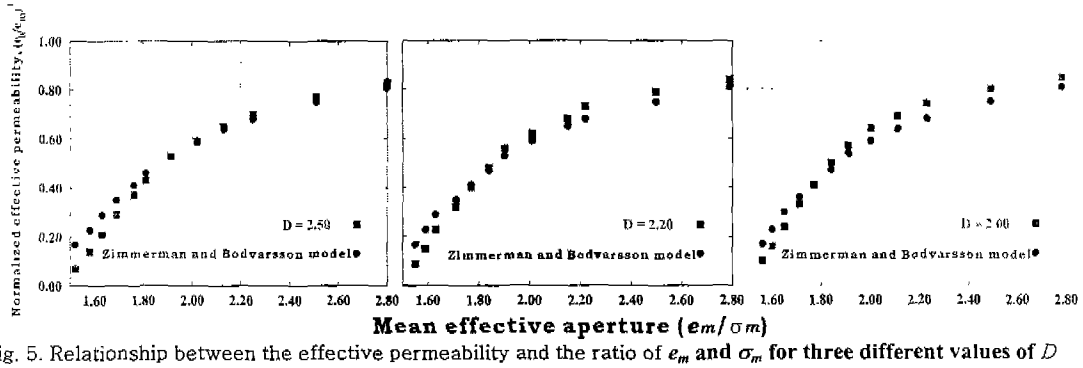

Fig. 5. Relationship between the effective permeability and the ratio of e_m and σ_m for three different values of D = 2.5, 2.2 and 2.0, and comparison with Zimmerman and Bodvarsson's empirical model.

The decreasing tendencies of effective permeability for three values of D = 2.5, 2.2 and 2.0 are almost

the same as those predicted by Zimmerman and Bodvarsson's model.

5.2 Solute transport simulations

Solute transport simulations were also carried out with the same fracture as that used in the fluid flow simulations. These simulations were performed in 10 independent distributions of apertures at each level of effective normal stress for two different values of D = 2.50 and 2.20. All of results obtained represents mean values of these 10 realizations.

Fig. 6 shows the variation of mean transit time of particles with the effective normal stress for D = 2.50 and 2.20. The mean transit time increases non-linearly with the effective normal stress. Moreover, the case of D = 2.50 increases slightly faster than that of D = 2.20. This result is due to the fact that the particle pathway in the fracture with D = 2.5 is more tortuous than that in the fracture with D = 2.20 (Fig.7).

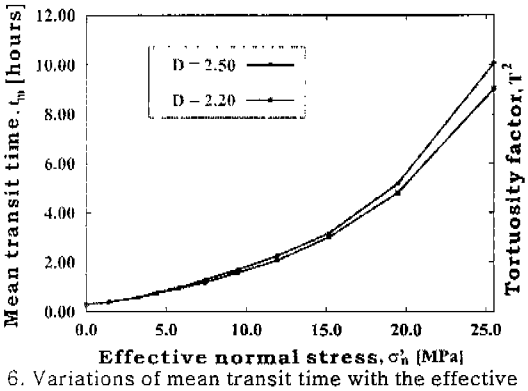

Fig. 6. Variations of mean transit time with the effective normal stress for D = 2.50 and 2.20.

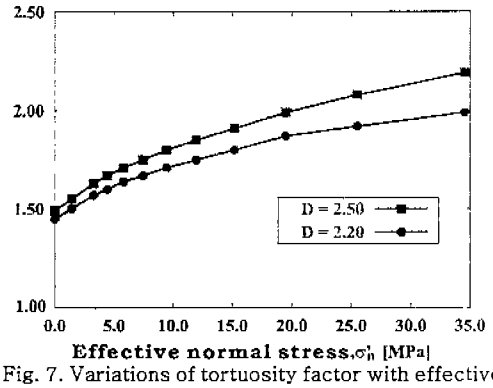

Fig. 7. Variations of tortuosity factor with effective normal stress for D = 2.50 and 2.20.

Fig. 8 illustrates the trajectories of particles transported along the most efficient channels for fluid flow. These channels are varied with the effective normal stress. This phenomenon is due to the increment of zones in contact by the effective normal stress and is similar to that obtained from David's work (1993).

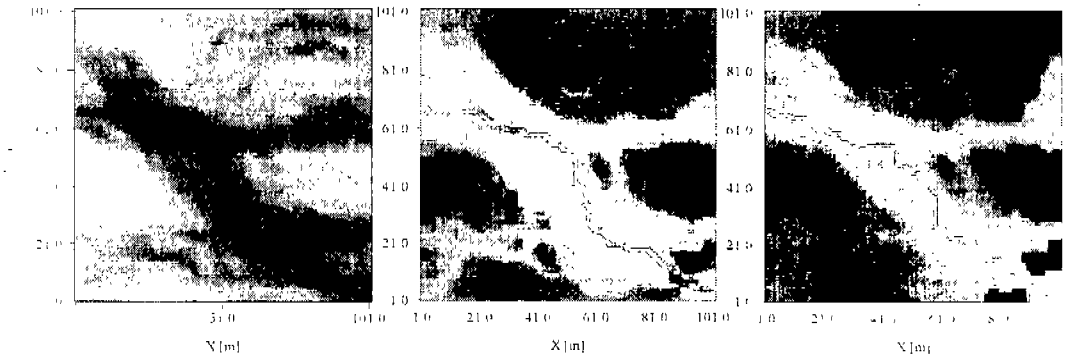

Fig. 8. Trajectories of particles transported along the most efficient channels for fluid flow at three different values of the effective normal stress. From left, σ'_n = **0.00, 15.18 and 25.50** ***MPa.***

Fig. 9 shows the variation of the Peclet number with the effective normal stress. This number is a dimensionless measure of the dispersivity (Moreno *et al.*, 1988) and is calculated by the same method as that performed by Moreno *et al.* (1988). We can see that there is no apparent difference between D = 2.50 and 2.20. The number of Peclet decreases very rapidly up to 5.80 *MPa* of σ'_n. This result means that the channels provided to particles are progressively reduced by zones in contact increasing as σ'_n increases. After this process, most of particles displace only along one or two main channels.

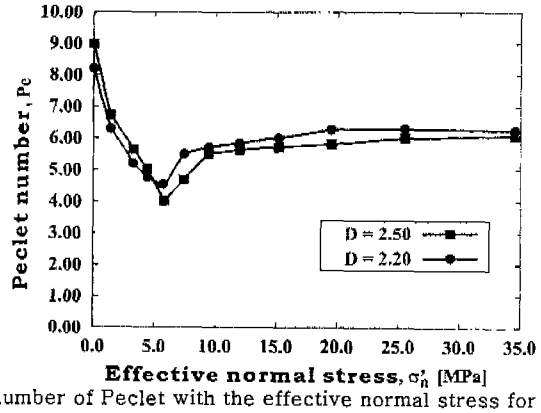

Fig. 9. Variations of number of Peclet with the effective normal stress for D = 2.50 and 2.20.

6. Conclusion

We studied numerically the hydromechanical behaviors of a single fracture generated by the self-affine fractal model and observed that the effective permeability of this fracture depends strongly on the distribution of variable aperture which is varied with the effective normal stress. The results obtained from these fluid flow simulations are a good agreement with those predicted by Zimmerman and Bodvarsson's empirical model. In the solute transport simulation, the most efficient channels for fluid flow are varied with the effective normal stress. However, once the effective normal stress arrives at certain level (*i.e.* 11.95 *MPa* in our study), these channels have almost the same form. Moreover, the particles displace only along the channel reduced and thus the spatial dispersion of particles become constant.

References

Hakami, E. and N. Barton (1990), "Aperture measurements and flow experiments using transparent replicas", In Barton N. and O. Stephansson (eds.), Rock Joints, Proc. Intern. Symp., Leon, Norway, 4-6 June, Rotterdam, Balkema

Bandis, S. C., A. C. Lumsden and N. R. Barton (1983), "Fundamentals of rock joint deformation", Int. J. Rock Mech. Min. Sci. & Geomech. Abstr., Vol. 20, No. 6, pp. 249-268

Brown, S. R. (1987), "Fluid flow through rock joints: The effect of surface roughness", Journal of Geophysical Research, Vol. 92, No. B2, pp. 1337-1347

Ewing, P. R. and D. B. Jaynes (1995), "Issues in single-fracture transport modeling: Scales, algorithms, and grid types", Water Resources Research, Vol. 31, No. 2, pp. 303-312

Gentier, S. (1986), "Morphologie et comportement hydromécanique d'une fracture naturelle dans un granite sous contrainte normale : étude expéimentale et théorique", Ph. D. Dissertation, Université d'Orléns, France

Jeong, Woo-Chang and Song Jai-Woo (1998), "Fluid Flow and Solute Transport in a Discrete Fracture Network Model with Nonlinear Hydromechanical Effect", Journal of Korea Water Resources Association, Vol. 31, No. 3

Meakin, P., T. Rage, G. Wagner, J. Feder and T. Jossang (1997), "Simulations of One- and Two-Phase Flow in Fractures", in Fluid Flow and Transport in Rocks, Chapman & Hall

Moreno, L., C. F. Tsang, Y. Tsang, F. V. Hale and I. Neretnieks (1988), "Flow and tracer transport in a single fracture: A stochastic model and its relation to some field observations", Water Resources Research, Vol. 24, No. 12, pp. 2033-2048

Pyrak-Nolte, L. J., N. G. W. Cook and D. D. Nolte (1988), "Fluid percolation through single fractures", Geophysics Research Letters, Vol. 15, No. 11, pp. 1247-1250

Renshaw, C. E. (1995), "On the relationship between mechanical and hydraulic apertures in rough-walled fractures", Journal of Geophysical Research, Vol. 100, No. B2, pp. 24629-24636

Thompson, M. E. (1991), "Numerical simulation of solute transport in rough fractures", Journal of Geophysical research, Vol. 96, No. B3, pp. 4157-4166

Zimmerman, R. W. and G. S. Bodvarsson (1996), "Hydraulic conductivity of rock fractures", Transport in Porous Media, No. 23, pp. 1-30